Wind and Structures, *Vol. 21, No. 2 (2015) 183-202*
DOI: http://dx.doi.org/10.12989/was.2015.21.2.183

Experimental investigation of Reynolds number effects on 2D rectangular prisms with various side ratios and rounded corners

Xinrong Wang and Ming Gu*

State Key Laboratory for Disaster Reduction in Civil Engineering, Tongji University, Shanghai 200092, China

(Received December 12, 2014, Revised May 8, 2015, Accepted June 16, 2015)

Abstract. Experiments on two-dimensional rectangular prisms with various side ratios (*B/D*=2, 3, and 4, where *B* is the along-wind dimension, and *D* is the across-wind dimension) and rounded corners (*R/D*=0%, 5%, 10%, and 15%, where *R* is the corner radius) are reported in this study. The tests were conducted in low-turbulence uniform flow to measure the wind pressures on the surfaces of 12 models for Reynolds numbers ranging from 1.1×10^5 to 6.8×10^5. The aerodynamic force coefficients were obtained by integrating the wind pressure coefficients around the model surface. Experimental results of wind pressure distributions, aerodynamic force coefficients, and Strouhal numbers are presented for the 12 models. The mechanisms of the Reynolds number effects are revealed by analyzing the variations of wind pressure distributions. The sensitivity of aerodynamic behavior to the Reynolds number increases with increasing side ratio or rounded corner ratio for rectangular prisms. In addition, the variations of the mean pressure distributions and the pressure correlations on the side surfaces of rectangular prisms with the rounded corner ratio are analyzed at $Re=3.4\times10^5$.

Keywords: wind tunnel test; Reynolds number effects; 2D rectangular prism; rounded corner; side ratio

1. Introduction

The corner modification of cross-sections of tall buildings has become a major aerodynamic measure that is commonly used in design practice. A few studies have verified that the introduction of corner modification often causes significant reductions in both the along-wind and cross-wind forces (Kwok *et al.* 1988, Kwok 1988, Tamura *et al.* 1998, Tamura and Miyagi 1999, Wang *et al.* 2003, Gu and Quan 2004, Irwin 2008, Xie 2014). Such reductions are helpful for modern building design practice. However, corner modification may produce a more complex flow around the body. Investigating the variation mechanisms of aerodynamic characteristics becomes more difficult for the bodies with various corner shapes. Moreover, compared with the case of sharp-edged models, the aerodynamic behaviors of models with corner modifications may be more dependent on test conditions, such as Reynolds number and turbulence of incoming flow (Delany and Sorensen 1953, Tamura *et al.* 1998, Tamura and Miyagi 1999, Larose and D'Auteuil, 2006, 2008, Carassale *et al.* 2013, 2014). This condition may increase the difficulty encountered by wind engineers in the design stage.

*Corresponding author, Professor, E-mail: minggu@tongji.edu.cn

http://www.techno-press.org/?journal=was&subpage=8 ISSN: 1226-6116 (Print), 1598-6225 (Online)

Several investigations have been conducted to investigate the effects of the corner modifications on the aerodynamic characteristics of building models. The pioneering study conducted by Delany and Sorensen (1953) showed that a sudden drop in drag coefficient is observed around the Reynolds number of 1.0×10^6 for a 2:1 rectangular prism with a small rounded corner (*R/D*=4%). Wind tunnel tests conducted by Kwok (1988) showed that slotted corners and chamfered corners produce significant reductions in both the along-wind and across-wind responses of a tall building model with a rectangular cross-section. Tamura *et al.* (1998, 1999) conducted wind tunnel tests to investigate the effect of the corner modification on the aerodynamic forces of two-dimensional (2D) and three-dimensional square cylinders in smooth and turbulent flow. A numerical simulation was also conducted in smooth flow. The results showed that chamfered and rounded corners decrease drag force because of the reduction in wake width. The mechanisms of aerodynamic force reduction were also clarified by the numerical simulation results. Furthermore, it is found that the shear layer that is separated from the leading edge reattached to the side surfaces of the corner-rounded cylinder in turbulent flow.

Larose and D'Auteuil (2006, 2008) conducted wind tunnel tests to investigate the effects of square edges, small chamfer, and large chamfer on aerodynamic coefficients of 2D rectangular prisms with side ratios of 2, 3, and 4 for the Reynolds numbers ranging from 0.3×10^6 to 2.5×10^6. The results showed that lift coefficients are apparently more sensitive to the Reynolds number than the drag coefficients, and the side ratio has a significant effect on the sensitivity of the lift coefficient to the Reynolds number. The development of the boundary layer on the model surface was affected by the presence of chamfer corners, which influenced the flow reattachment on the side surface of the body and the sensitivity of aerodynamic coefficients to the Reynolds number.

Experiments (Carassale *et al.* 2013, 2014) were then conducted to measure the aerodynamic forces and the wind pressures of square cylinders with sharp-edge corner and two different rounded corner ratios (*R/D*=1/15 and 2/15) at Reynolds numbers ranging between 1.7×10^4 and 2.3×10^5. The rounded corner results in a reduction in the critical angle of incidence for which the flow reattaches to the lateral face exposed to wind. Moreover, the Reynolds number effects on the square cylinder with the rounded corner ratio *R/D*=2/15 are observed because of the presence of transition phenomena involving flow reattachment on the lateral faces and the potentially unstable range of angle shifts with the Reynolds number in turbulent flow.

A series of wind tunnel experiments (Tanaka *et al.* 2012, Tamura *et al.* 2013) were recently conducted to determine the aerodynamic forces and wind pressures acting on tall building models with various configurations. The experimental results can be used to evaluate the most effective structural shape in wind-resistant design for various tall buildings.

As previously demonstrated, the aerodynamic characteristics of the square cylinder may drastically change with slight changes in corner shape (Tamura *et al.* 1998). The rounded corners may cause the absence of the fixed flow separation point, which influences the formation of the separated shear layer at the leading edge. Thus, the presence or the extent of the flow reattachment regions may also be affected. This brief review shows that previous research mainly aimed at the effects of modified corners, such as rounded corners, chamfered corners, and concave corners, on the aerodynamic forces for square buildings. Studies on the Reynolds number effects on rectangular prisms with various corner shapes are relatively few, but have attracted increasing attention in recent years. Meanwhile, wind pressure correlations on the surface of the rectangular prisms with various corner shapes have received limited attention, especially for the wind pressure correlations on the side surfaces of the bodies that may be obviously influenced by the presence of the flow reattachment.

This research systematically investigates the Reynolds number effects on the aerodynamic characteristics of 2D rectangular prisms with various side ratios (*B/D*=2, 3, and 4) and rounded corners (*R/D*=0%, 5%, 10%, and 15%). The testing Reynolds numbers are from 1.1×10^5 to 6.8×10^5, which correspond to the variance of the Reynolds number from the subcritical range to the supercritical range for a 2D circular cylinder. The experimental results of wind pressure distributions, aerodynamic force coefficients, and Strouhal numbers are presented for 12 models. The mechanisms of the Reynolds number effects are revealed by analyzing the variations of wind pressure distributions. In addition, the effects of the rounded corners on the pressure correlations and the wind pressure distributions on the side surfaces of the models are analyzed at $Re=3.4\times10^5$.

2. Experimental details

2.1 Model details and experimental facilities

The experiments were conducted in smooth flow in the TJ-2 Boundary Layer Wind Tunnel at Tongji University, the working section of which is 3 m wide and 2.5 m high. The wind fields adopted in the experiments had uniform flow with low turbulence levels. The turbulence intensity at the model location was approximately 1% when the wind speed reached 10 m/s and was less than 0.5% when the wind speed exceeded 15 m/s.

Fig. 1 shows the corner rounding modification of the rectangular prism. The rounded corner ratio *R/D* refers to the ratio of the corner radius *R* to the across-wind dimension *D*. The side ratio *B/D* refers to the ratio of the along-wind dimension *B* to the across-wind dimension *D*. Fig. 2 shows the cross-sectional dimensions of the 2D rectangular prisms selected for this study. The side ratio (*B/D*) varies from 2 to 4, whereas the rounded corner ratio (*R/D*) varies from 0% to 15%.

The length and the across-wind dimension *D* of all models were 1.5 and 0.2 m, respectively. Therefore, the aspect ratio and the blockage ratio were 7.5 and 4%, and effects of the blockage on experimental results were not considered in the present study. The testing wind speed ranged from 8 m/s to 50 m/s, and the Reynolds numbers were from 1.1×10^5 to 6.8×10^5 based on $D = 0.2$ m. All models were symmetric in both the streamwise direction and the vertical axis.

Two sets of pressure taps were arranged on the surface of each model. One set was around the circumference of the cross-section at the mid-span. The maximum spacing of pressure taps was 20 mm at the central area of the side surfaces, and the minimum spacing of pressure taps was 5 mm close to the corners of the model. Taking the 3:1 rectangular prism with *R/D* = 0% as an example, there were 120 pressure taps in the circumferential measurement line at the mid-span. The second set of pressure taps was in the spanwise centerlines of the windward and leeward sides of the model, and 29 pressure taps were arranged in each centreline with a constant spacing of 50 mm. The DSM3000 electronic pressure scan valve system was used to measure the wind pressures acting on the models. The sampling frequency was 312.5 Hz, whereas the measuring duration was 28.8 s. The pressure measurements were corrected for pressure signal distortion, both in magnitude and phase, because of the pneumatic tubing with 0.5 mm internal diameter and 0.8 m length.

All models were made of 7 mm thick organic glass to maintain smooth and flat surfaces. Each model was supported by a steel frame and mounted on the horizontal and vertical centers of the tunnel cross-section, and the steel frame had sufficient strength and rigidity to ensure experimental accuracy under the condition of high wind speeds. Fig. 3 shows the photograph of the test setup and model.

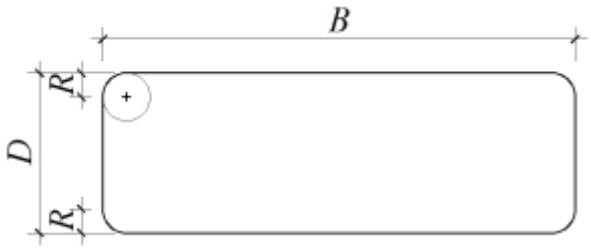

Fig. 1 Sketch of rounded corner modification

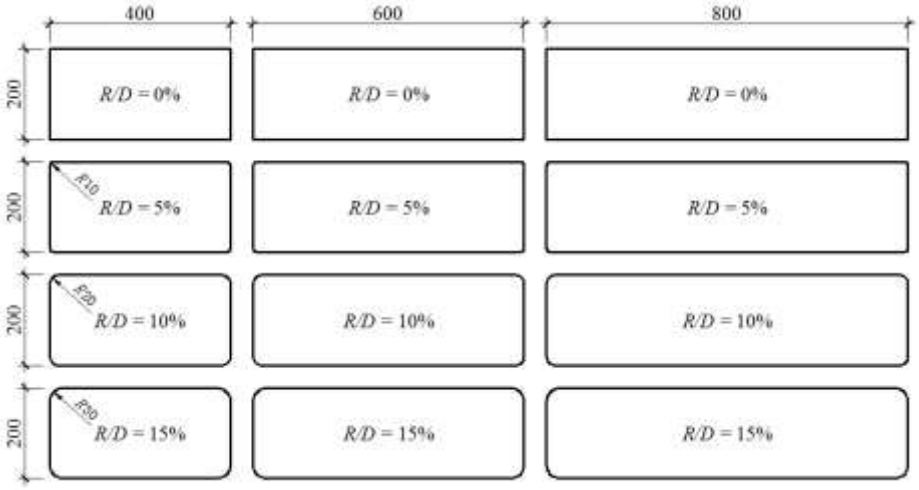

Fig. 2 Sketches of the cross-sectional dimensions of models (Units: mm)

Fig. 3 View from upstream of the sectional model installed in the wind tunnel

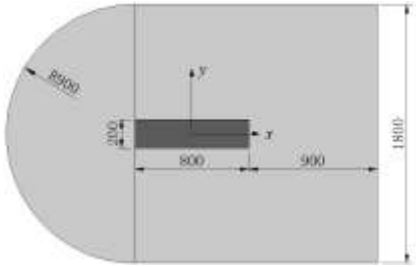

Fig. 4 Size of the end plate (Units: mm)

2.2 2D flow around the testing models

2D models were adopted for this experiment, and the production of 2D flow around the testing bodies determined the reliability of experimental data. According to the study by Kubo *et al.* (1989), the required size of the end plates is related to the size of the wake, which can be calculated by Karman's theory of vortex streets. The size of the end plates adopted for this experiment is shown in Fig. 4. The end plates were made of 8 mm thick aluminum to meet the test requirements of strength and rigidity. The leading edges of the end plates were chamfered to decrease the width of the wake flow, which can reduce the influence of wake flow on the testing models.

Two rows of pressure taps in the spanwise centerlines of the windward and leeward sides of each model were arranged to monitor the 2D flow around testing models. Fig. 5 shows the mean pressure distributions ($C_{p\ mean}$) along the length of the rectangular prisms with side ratios of 2 and 4 at various Reynolds numbers. Notably, the mean pressure coefficients on the windward sides of two models were approximately 1.0 at various Reynolds numbers, and the mean pressure coefficients on the leeward side of each model slightly varied with the Reynolds number. However, the mean pressure coefficients remained almost unchanged along the length of each model at the same Reynolds number. This phenomenon proves that the flow around each testing model remains unchanged along the length of the model. Therefore, the 2D flow around the testing bodies can satisfactorily fulfill the test requirements.

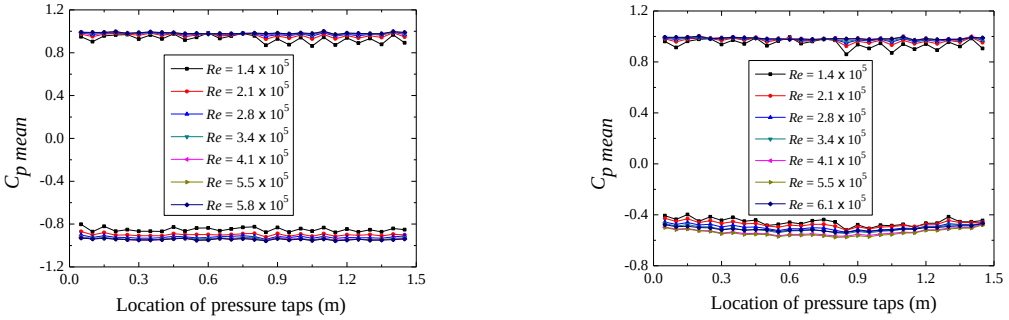

(a) *B*/*D*=2 (b) *B*/*D*=4

Fig. 5 Variation of mean pressure coefficient along the length of the model

3. Data processing methods

The time history of the wind pressure coefficients at pressure tap *i* is calculated as follows

$$C_p(i,\mathrm{t}) = \frac{P_i - P_\infty}{(1/2)\rho \mathrm{U}^2} \tag{1}$$

where P_i is the actual pressure measured at the pressure tap i; P_∞ is the reference static pressure; and ρ and U are the air density and the wind velocity, respectively. Aerodynamic forces (drag and lift) are obtained by integrating the wind pressures around the model surface (neglecting viscous drag).

$$C_D(t) = \frac{F_x(t)}{(1/2)\rho U_0^{\,2} D} = \frac{1}{D}\sum_i C_P(i,t)\cdot \Delta S_i \cdot \cos\theta_i \tag{2}$$

$$C_L(t) = \frac{F_y(t)}{(1/2)\rho U_0^{\,2} D} = \frac{1}{D}\sum_i C_P(i,t)\cdot \Delta S_i \cdot \sin\theta_i \tag{3}$$

where D is the across-wind dimension, ΔS_i represents the width on the model surface belonging to the pressure tap i, and θ_i is the angle between wind pressure and wind velocity (see Fig. 6).

The Strouhal number is defined as follows

$$St = f \cdot D/U \tag{4}$$

where f is the frequency corresponding to the obvious peak in the power spectrum of fluctuating lift force. The pressure correlation coefficient is defined as follows

$$R(C_{pi}, C_{pj}) = \frac{\mathrm{cov}(C_{pi}, C_{pj})}{\sigma_{C_{pi}} \cdot \sigma_{C_{pj}}} \tag{5}$$

where cov (C_{pi} , C_{pj}) is the covariance between C_{pi} and C_{pj}, whereas $\sigma_{C_{pi}}$ is the standard deviation of C_{pi}.

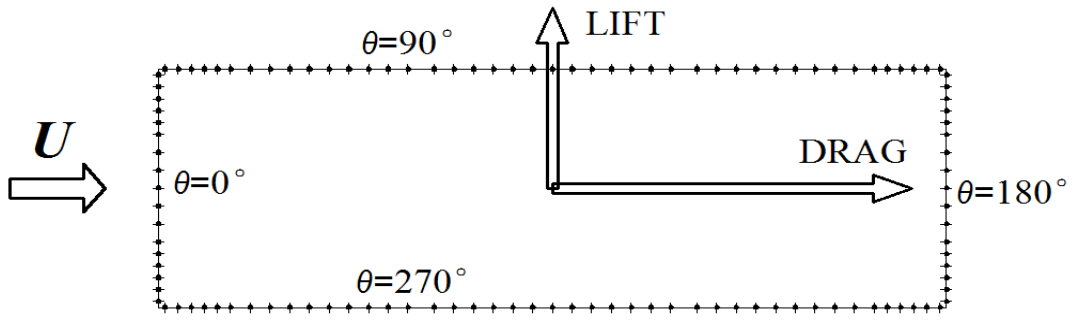

Fig. 6 Sketch of the drag and lift force

4. Main results

4.1 Wind pressure distribution

The wind pressure distributions of rectangular prisms contain a wealth of information, and the mechanisms of the Reynolds number effects can be determined by analyzing the variations of wind pressure distributions. Previous experimental results showed that flow around the sharp-edged rectangular prisms are influenced by the Reynolds number which is related to the flow reattachment on the side surface of the prisms (Robertson *et al.* 1975). With increasing the side ratio, rectangular prisms have a possibility of flow reattachment on the side surface, which may increase the sensitivity of their aerodynamic characteristics to the Reynolds number. Meanwhile, with increasing the rounded corner ratio, the separated flow can reattach to the side surface with ease. Therefore, rectangular prisms may be more sensitive to the Reynolds number with increasing side ratio or rounded corner ratio.

The mean pressure distributions ($C_{p\ mean}$) around 12 rectangular prisms at various Reynolds numbers are presented in Fig. 7. The discontinuities on the mean pressure distributions at low Reynolds numbers (e.g. $Re \approx 1.4 \times 10^5$) are not related to the aerodynamic characteristics of the model, and these discontiunities are the instrumental error of the electronic pressure scan value system under the condition of the low wind velocity. The mean pressure distributions on the side surfaces of the 2:1 rectangular prism with R/D = 0% do not exhibit a pressure increase toward the trailing edge, and a little pressure recovery on the side surfaces of the 2:1 rectangular prism with R/D = 5% is observed, whereas the mean pressure distributions on the side surfaces of the other 10 rectangular prisms manifest obvious pressure recoveries. Lacking of complete pressure recovery near the trailing edge of the side surface indicates that the separated flow does not reattach to the side surfaces of the model. Therefore, the 2:1 rectangular prisms with R/D = 0% and 5% does not exhibit complete flow reattachment, whereas the other 10 rectangular prisms exhibit complete flow reattachment. Furthermore, for each kind of side ratio, four rectangular prisms with various rounded corners can be classified into two categories according to the variations of wind pressure distributions with the Reynolds number. These two categories are rectangular prisms with R/D = 0% and 5% and those with R/D = 10% and 15%. Compared with those of the models with R/D = 0% and 5%, the wind pressure distributions of the models with R/D = 10% and 15% are sensitive to the Reynolds number, when $Re \approx 5.4 \times 10^5$.

For the 2:1 rectangular prisms with R/D = 0% and 5% (see Figs. 7(a) and 7(d)), the negative pressures on side surfaces increase with the Reynolds number, even if the flow does not reattach to the side surfaces. For the 2:1 rectangular prisms with R/D = 10% and 15% (see Figs. 7(g) and 7(j)), with increasing Reynolds number, the negative pressures in the separation bubble near the leading edge increase, whereas the negative pressures in the flow reattachment region gradually decrease. In addition, the flow reattachment point moves steadily toward the leading edge.

For the 3:1 rectangular prisms with R/D = 0% and 5% (see Figs. 7(b) and 7(e)), the Reynolds number influences the mean pressures only in the separation bubble near the leading edge, but not in the flow reattachment region. For the 3:1 rectangular prisms with R/D = 10% and 15% (see Figs. 7(h) and 7(k)), a significant influence of the Reynolds number on the mean pressure distributions is observed. These two models exhibit similar behavior characterized by the sudden change in mean pressure distributions at a critical Reynolds number. When the Reynolds number reaches 5.4×10^5, the negative pressures in the separation bubble suddenly increase, whereas the negative pressures in the flow reattachment region suddenly decrease. Moreover, the location of the flow

reattachment moves toward the leading edge accordingly.

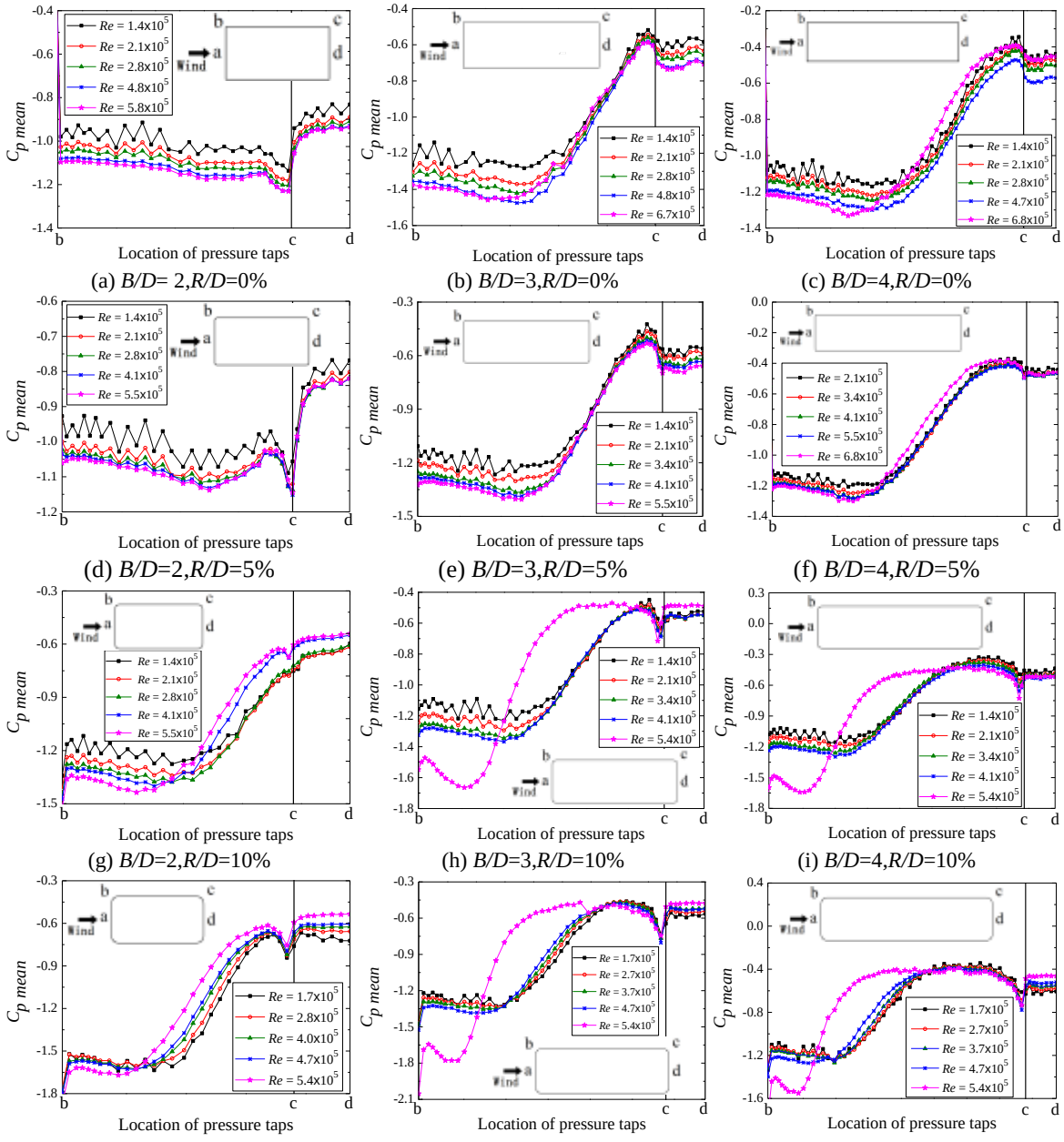

(a) *B/D*= 2,*R/D*=0% (b) *B/D*=3,*R/D*=0% (c) *B/D*=4,*R/D*=0%

(d) *B/D*=2,*R/D*=5% (e) *B/D*=3,*R/D*=5% (f) *B/D*=4,*R/D*=5%

(g) *B/D*=2,*R/D*=10% (h) *B/D*=3,*R/D*=10% (i) *B/D*=4,*R/D*=10%

(j) *B/D*=2,*R/D*=15% (k) *B/D*=3,*R/D*=15% (l) *B/D*=4,*R/D*=15%

Fig. 7 Mean pressure distributions around rectangular prisms at various Reynolds numbers

For the 4:1 rectangular prisms with *R/D* = 0% and 5% (see Figs. 7(c) and 7(f)), as the Reynolds number increases, the negative pressures in the separation bubble near the leading edge gradually increase, whereas the negative pressures in the flow reattachment region initially increase and then suddenly decrease at $Re \approx 6.8 \times 10^5$. For the 4:1 rectangular prisms with *R/D* = 10% and 15% (see Figs. 7(i) and 7(l)), the Reynolds number effects on the mean pressure distributions of these two models are similar to those in the case of 3:1 rectangular prisms with *R/D* = 10% and 15% (see Figs. 7(h) and 7(k)). Thus, the results will no longer be discussed here.

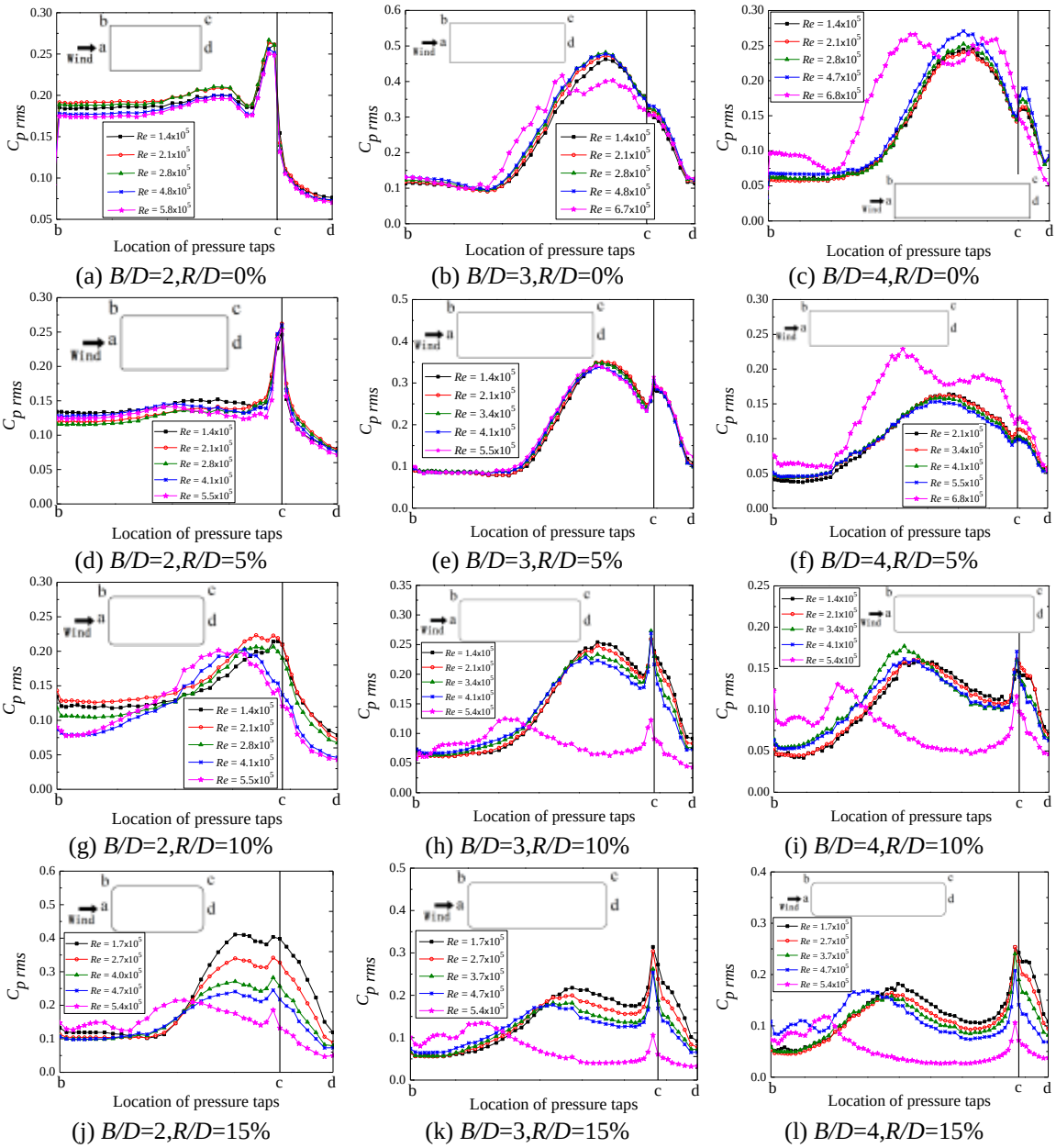

(a) *B/D*=2,*R/D*=0% (b) *B/D*=3,*R/D*=0% (c) *B/D*=4,*R/D*=0%

(d) *B/D*=2,*R/D*=5% (e) *B/D*=3,*R/D*=5% (f) *B/D*=4,*R/D*=5%

(g) *B/D*=2,*R/D*=10% (h) *B/D*=3,*R/D*=10% (i) *B/D*=4,*R/D*=10%

(j) *B/D*=2,*R/D*=15% (k) *B/D*=3,*R/D*=15% (l) *B/D*=4,*R/D*=15%

Fig. 8 Fluctuating pressure distributions around rectangular prisms at various Reynolds numbers

Fig. 8 shows the fluctuating pressure distributions ($C_{p\ rms}$) around 12 rectangular prisms at various Reynolds numbers. For the 2:1 rectangular prisms with $R/D \leq 5\%$ (see Figs. 8(a) and 8(d)) and the 3:1 rectangular prisms with $R/D \leq 5\%$ (see Figs. 8(b) and 8(e)), no significant influence of the Reynolds number is found. However, the fluctuating pressure distributions of the 4:1 rectangular prisms with $R/D \leq 5\%$ are obviously changed at $Re \approx 6.8\times10^5$ (see Figs. 8(c) and 8(f)).

For the 2:1 rectangular prisms with R/D=10% and 15% (see Figs. 8(g) and 8(j)), as the Reynolds number increases, peaks of the fluctuating pressures in the flow reattachment region gradually decrease, similar to the fluctuating pressures on the leeward sides of the bodies. For the 3:1 rectangular prisms with R/D=10% and 15% (see Figs. 8(h) and 8(k)) and the 4:1 rectangular prisms with R/D=10% and 15% (see Figs. 8(i) and 8(l)), obvious peaks of the fluctuating pressure distributions are observed at the rounded corners near the trailing edge, and the peaks significantly reduce at a Reynolds number of 5.4×10^5.

4.2 Aerodynamic force coefficients

4.2.1 Mean drag coefficients

Fig. 9 shows the variations of the mean drag coefficients ($C_{D\ mean}$) with the Reynolds number for 12 rectangular prisms. For the 2:1 rectangular prisms with R/D=0% and 5%, a gradual increase of the mean drag coefficients is observed with increasing Reynolds number from 1.1×10^5 to 3.0×10^5, which is followed by a plateau up to 6.0×10^5. For the 2:1 rectangular prisms with R/D=10% and 15%, sudden decreases of the mean drag coefficients are observed at $Re \approx 4.0\times10^5$ and 5.0×10^5(see Fig. 9(a)).

For the 3:1 rectangular prisms (see Fig. 9(b)), the mean drag coefficients of the models with R/D=0% and 5% gradually increase with Reynolds number ranging from 1.1×10^5 to 6.0×10^5, whereas sudden jumps of the mean drag coefficients are observed for rectangular prisms with R/D=10% and 15% at $Re \approx 4.1\times10^5$ and 5.0×10^5.

For the 4:1 rectangular prisms (see Fig. 9(c)), the mean drag coefficients of the model with R/D=0% steadily increase with Reynolds number ranging from 1.1×10^5 to $5.0\times10^5$and then rapidly decrease when the Reynolds number is greater than approximately 5.0×10^5. The mean drag coefficients of the models with R/D=5% and 10% slightly increase with increasing Reynolds number from 1.1×10^5 to 6.0×10^5. For the model with R/D=15%, a significant effect of the Reynolds number on the mean drag coefficients is observed, especially with Reynolds number ranging from 4.0×10^5 to 6.0×10^5.

According to the above analysis, the mean drag coefficients of rectangular prisms appear to be more sensitive to the Reynolds number with increasing rounded corner ratios. This phenomenon can be attributed to the fact that rectangular prisms are transformed from bluff bodies to streamlined bodies by the corner rounding modification, such that the flow reattachment occurs with ease. In addition, for the rectangular prisms with B/D=2 and 3, the mean drag coefficients decrease with increasing rounded corner ratio. In fact, the presence or the extent of the flow reattachment regions is again the reason for the decrease in the mean drag coefficients with the rounded corner ratio. With increasing rounded corner ratio, the shear layer that is separated from the leading edge reattaches to the side surface with ease, thus resulting in a reduction in wake width.

4.2.2 RMS drag coefficients

Fig. 10 shows the variations of the RMS drag coefficients ($C_{D\ rms}$) with the Reynolds number

for 12 rectangular prisms. For the 2:1 rectangular prisms with *R/D*=0% and 5%, a gradual decrease of the RMS drag coefficients is observed with Reynolds number ranging from 1.0×10^5 to 2.0×10^5. This decrease is followed by a plateau up to 6.0×10^5. For the 2:1 rectangular prisms with *R/D*=10% and 15%, significant decreases of the RMS drag coefficients are observed when the Reynolds number is greater than approximately 3.0×10^5 and 5.0×10^5, respectively (see Fig. 10(a)). No significant influences of the Reynolds number on the RMS drag coefficients are found for the 3:1 rectangular prisms with *R/D*=0% and 5%, whereas obvious decreases of the RMS drag coefficients are observed for the 3:1 rectangular prisms with *R/D*=10% and 15% at $Re>4.0\times10^5$(see Fig. 10(b)). For the 4:1 rectangular prisms with *R/D*=0%, 5%, and 10%, Reynolds number effects on the RMS drag coefficients are not obvious. However, the RMS drag coefficients of the 4:1 rectangular prisms with *R/D*=15% gradually decrease with the Reynolds number (see Fig. 10(c)).

4.2.3 RMS lift coefficients

The values of the mean lift coefficients are approximately zero because the rectangular prisms selected for the experiments are symmetric in the streamwise direction, and no Reynolds number effects on the mean lift coefficients are observed. However, the values of the RMS lift coefficients for rectangular prisms with various rounded corners are influenced by the Reynolds number. Fig. 11 shows the variations of the RMS lift coefficients ($C_{F\ rms}$) of all models with the Reynolds number. Compared with rectangular prisms with *R/D*=0% and 5%, the RMS lift coefficients of the models with *R/D* = 10% and 15% are more sensitive to the Reynolds number.

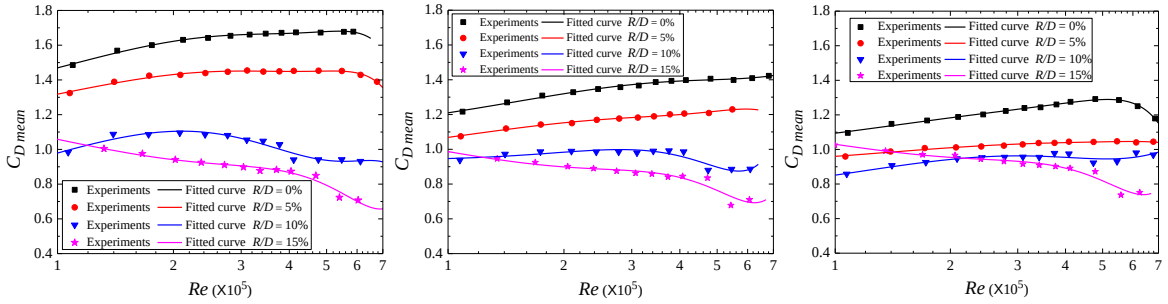

(a) *B/D*=2 (b) *B/D*=3 (c) *B/D*=4

Fig. 9 Variation of the mean drag coefficients with the Reynolds number

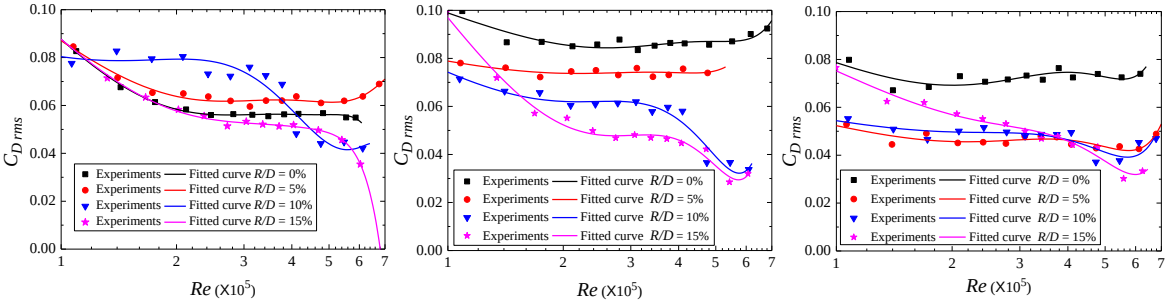

(a) *B/D*=2 (b) *B/D*=3 (c) *B/D*=4

Fig. 10 Variation of the RMS drag coefficients with the Reynolds number

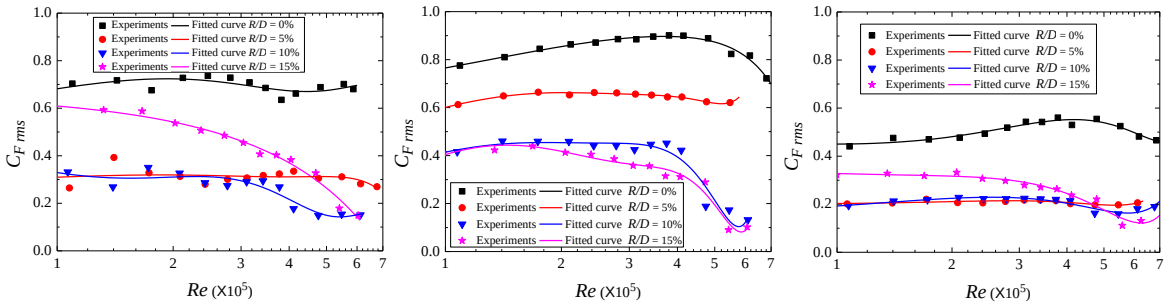

(a) *B/D*=2 (b) *B/D*=3 (c) *B/D*=4

Fig. 11 Variation of the RMS lift coefficients with the Reynolds number

For the 2:1 rectangular prisms, Reynolds number effects on the RMS lift coefficients are not obvious for the models with *R/D*=0% and 5%, whereas a gradual decrease of the RMS lift coefficients is observed for the 2:1 rectangular prism with *R/D*=15%. For the 2:1 rectangular prism with *R/D*=10%, a sudden decrease of the RMS lift coefficients is observed at $Re \approx 4.0\times10^5$(see Fig. 11(a)). For the 3:1 rectangular prism with *R/D*=0%, the RMS lift coefficients slowly increase with increasing Reynolds number to 4.0×10^5, after which the RMS lift coefficients declines. The RMS lift coefficients of the 3:1 rectangular prism with *R/D*=5% are not influenced by the Reynolds number. However, sudden decreases of the RMS lift coefficients are observed for the 3:1 rectangular prisms with *R/D*=10% and 15% at $Re \approx 4.1\times10^5$ and 5.0×10^5, respectively (see Fig. 11(b)). The Reynolds number effects on the RMS lift coefficients of the 4:1 rectangular prisms are similar to those on the 3:1 rectangular prisms. Reynolds number effects are significant on the RMS lift coefficients of the 4:1 rectangular prisms with *R/D*=10% and 15% (see Fig. 11(c)).

4.3 Lift force power spectrum and the Strouhal number

4.3.1 Lift force power spectrum

Figs. 12-14 show the power spectrum of the lift coefficients for 12 rectangular prisms at various Reynolds numbers. Notably, the lift force acting on the rectangular prisms is primarily caused by random vortex shedding, which can be confirmed by the peaks on the power spectrum curves. The Strouhal number is defined as the reduced frequency corresponding to the obvious peak in the power spectrum of fluctuating lift forces (Liang *et al.* 2002).

For the 2:1 rectangular prisms with *R/D*=0% and 15% (see Figs. 12(a) and 12(d)), sharp and narrow peaks are observed on the curves of the lift force power spectrum, and the bandwidth is small. However, for the 2:1 rectangular prisms with *R/D*=5% and 10% (see Figs. 12(b) and 12(c)), the bandwidth of the peaks is relatively broadened.

For the 3:1 rectangular prisms with *R/D*=0% and 5% (see Figs. 13(a) and 13(b)), narrow and sharp peaks are found on the curves of lift force power spectrum, and the reduced frequencies corresponding to the obvious peaks hardly changed with the Reynolds number. However, for the 3:1 rectangular prisms with *R/D*=10% and 15% (see Figs. 13(c) and 13(d)), the peaks on the curves of lift force power spectrum are obviously changed at high Reynolds number of 6.1×10^5.This phenomenon indicates that the regular vortex shedding tends to be disturbed, and the

bandwidth of the peaks is broadened without obvious sharp peaks.

The Reynolds number has an obvious effect on the lift force power spectrum for the 4:1 rectangular prisms with various rounded corners (see Fig. 14). When $Re \leq 4.8\times10^5$, narrow and obvious sharp peaks are observed on the power spectrum curves of four models, the corresponding reduced frequencies of which are Strouhal numbers. However, when $Re \approx 6.1\times10^5$, two peaks are found on the curves of the power spectrum for the 4:1 rectangular prisms with R/D=0% and 5%. For the 4:1 rectangular prisms with R/D=10% and 15%, the bandwidth of the peaks is obviously broadened at $Re \approx 6.1\times10^5$.

4.3.2 Strouhal number

Table 1 shows the value range of the Strouhal numbers for 12 rectangular prisms with Reynolds numbers ranging between 1.1×10^5 and 6.8×10^5. For the 2:1 rectangular prisms with various rounded corners, the Strouhal numbers hardly change with the Reynolds number. However, for the rectangular prisms with side ratios of 2 and 3, the variations of the Strouhal number are greater with increasing rounded corner ratio in the testing Reynolds number range. Notably, the Reynolds number has an obvious effect on the Strouhal number of the 3:1 rectangular prisms with $R/D \geq 10\%$ and 4:1 rectangular prisms with $R/D \geq 10\%$.

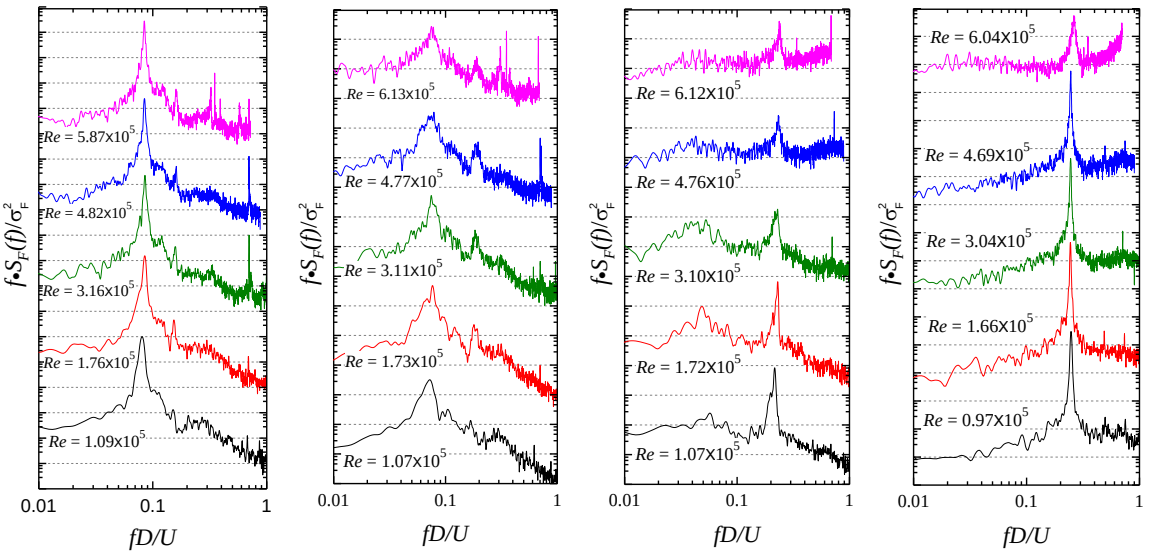

(a) R/D=0% (b) R/D=5% (c) R/D=10% (d) R/D=15%

Fig. 12 Power spectrum of lift coefficients for the 2:1 rectangular prisms at various Reynolds numbers

Table 1 Strouhal numbers of the 12 models

Rounded corner ratio	Strouhal number		
	B/D=2	B/D=3	B/D=4
R/D=0%	0.088~ 0.089	0.167~ 0.181	0.144~ 0.154
R/D=5%	0.072~ 0.079	0.176~ 0.192	0.159~ 0.176
R/D=10%	0.215~ 0.237	0.183~ 0.239	0.185~ 0.226
R/D=15%	0.245~ 0.264	0.209~ 0.272	0.208~ 0.265

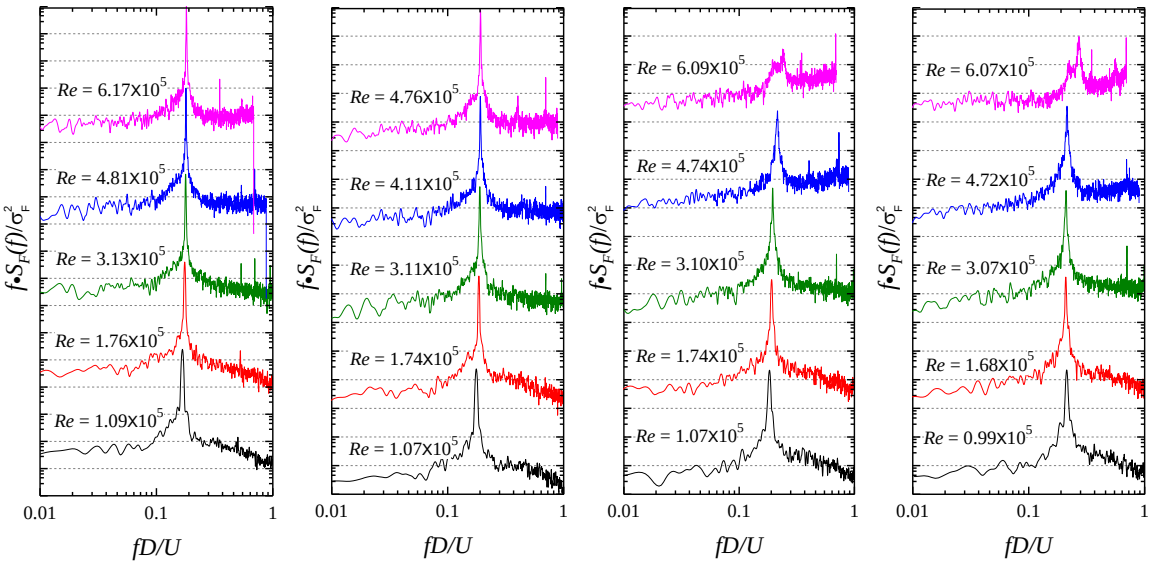

(a) *R/D*=0% (b) *R/D*=5% (c) *R/D*=10% (d) *R/D*=15%

Fig.13 Power spectrum of lift coefficients for the 3:1 rectangular prisms at various Reynolds numbers

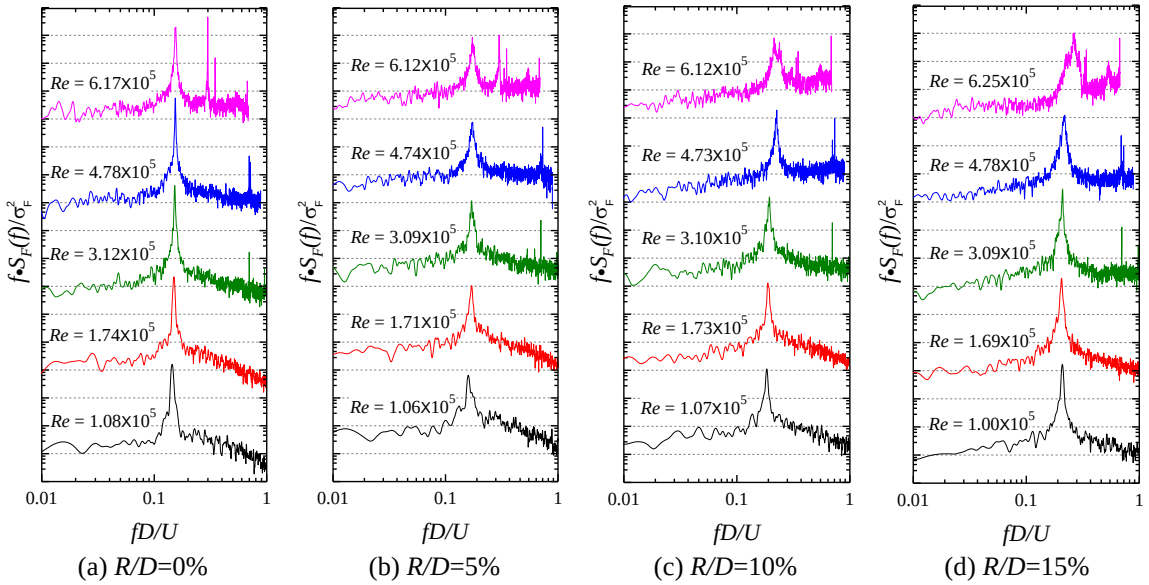

(a) *R/D*=0% (b) *R/D*=5% (c) *R/D*=10% (d) *R/D*=15%

Fig. 14 Power spectrum of lift coefficients for the 4:1 rectangular prisms at various Reynolds numbers

4.4 Pressure correlation coefficients

In this section, mean pressure distributions and pressure correlations on the side surfaces of 12 rectangular prisms are analyzed at Re=3.4×10^5, and the pressure correlation coefficients with

respect to three typical measuring points (Points A, B, and C) are respectively presented in Figs. 17, 19, and 21. Point A refers to the point near the leading edge, Point B refers to the midpoint at the side surface, and Point C refers to the point near the trailing edge. The X used in Figs. 16-21 is defined as the distance from the location of pressure taps to the leading edge. Taking the 3:1 rectangular prism with *R/D*=10% as an example, the locations of three typical measuring points and the definition of the X are shown in Fig. 15.

4.4.1 2:1 Rectangular prisms with various rounded corners

Fig. 16 presents the mean pressure distributions on the side surfaces of the 2:1 rectangular prisms with various rounded corners at $Re=3.4\times10^5$. Notably, the rounded corners have a significant effect on the mean pressure distributions on the side surfaces of four models. For the models with *R/D*=0% and 5%, the mean pressure coefficients on the side surfaces remain almost unchanged at −1.2 to -1.0 because the shear layer does not reattach to the side surfaces. However, judging from the variation of the mean pressure distribution, the 2:1 rectangular prisms with *R/D*=10% and 15% exhibit complete flow reattachment, and the flow reattachment point moves toward the leading edge with increasing rounded corner ratio. Compared with the model with *R/D*=10%, the negative pressures in the separation bubble of the model with *R/D*=15% significantly increase, whereas the negative pressures in the flow reattachment region of the model with *R/D*=15% obviously decrease.

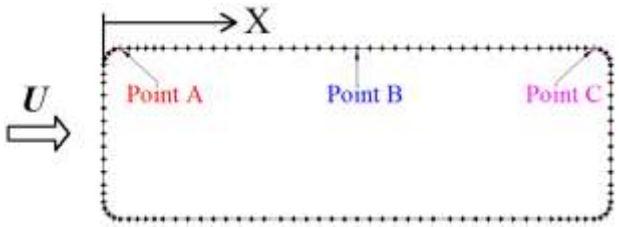

Fig. 15 Locations of the three points and the definition of the X

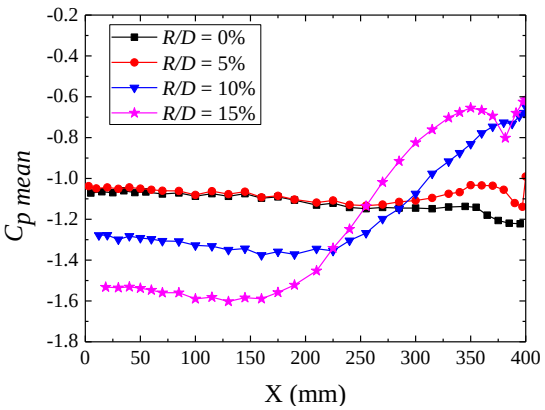

Fig. 16 Mean pressure distributions on the side surfaces of the 2:1 rectangular prisms with various rounded corners

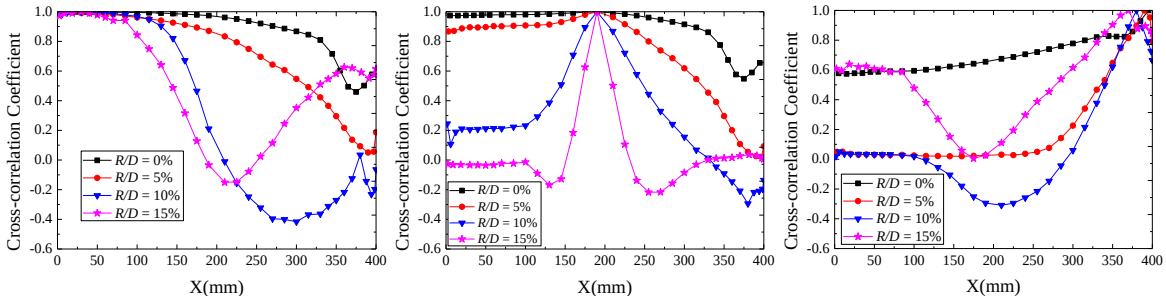

(a) Point A (b) Point B (c) Point C

Fig. 17 Pressure correlation coefficients on the side surfaces of the 2:1 rectangular prisms with respect to various points

Pressure correlations on the side surfaces of the 2:1 rectangular prisms with various rounded corners are analyzed at $Re = 3.4 \times 10^5$ (see Fig. 17). Figs. 17(a) and 17(c) present the pressure correlation coefficients with respect to Points A and C, respectively. For the models with R/D = 0% and 5%, pressure correlation coefficients decrease with increasing rounded corner ratio. However, for the models with R/D = 10% and 15%, wind pressures near the leading edge exhibit relatively good correlations with wind pressures near the trailing edge. In Fig. 17(b), good correlations of wind pressures are observed on the side surfaces of the models with R/D = 0% and 5%, and only a gradual decrease in the pressure correlation coefficients near the trailing edge is observed for the model with R/D = 5%. However, for the models with R/D = 10% and 15%, poor correlations are observed between the wind pressures near the midpoint of side surface and the wind pressures near the leading and trailing edges.

4.4.2 3:1 Rectangular prisms with various rounded corners

The effects of rounded corners on the mean pressure distributions on the side surfaces of the 3:1 rectangular prisms at $Re=3.4\times10^5$ are shown in Fig.18. Notably, the mean pressure distributions on the side surfaces are influenced by the rounded corners only in the flow reattachment region. The negative pressure in the separation bubble near the leading edge does not vary with the rounded corner ratios. With increasing rounded corner ratios, the negative pressures in the flow reattachment region gradually decrease, and the flow reattachment point moves steadily toward the leading edge.

The variations of the pressure correlations on the side surfaces of the 3:1 rectangular prisms with various rounded corners at $Re = 3.4 \times 10^5$ are presented in Fig. 19. Given the flow reattachment on the side surface of four models, good correlations are observed between the wind pressures near the leading edge and the trailing edge (see Figs. 19(a) and 19(c)). By contrast, the wind pressures near the midpoint of the side surface have poor correlations with the wind pressures near the leading edge and the trailing edge (see Fig. 19(b)). With increasing rounded corner ratio, the pressure correlations between Point A and the points in the separation bubble (X < 300 mm) increasingly weaken (see Fig. 19(a)). In addition, compared with the models with R/D = 5%, 10%, and 15%, a stronger pressure correlation is observed between Point C and the points in the separation bubble near the leading edge for the model with R/D = 0% (see Fig. 19(c)).

4.4.3 4:1 Rectangular prisms with various rounded corners

The effects of corner rounding modification on the mean pressure distributions and the pressure correlations on the side surfaces of the 4:1 rectangular prisms at Re=3.4×10^5 are shown in Figs. 20 and 21, respectively. The effects of rounded corners on the mean pressure distributions on the side surfaces of the 4:1 rectangular prisms are similar to those of the 3:1 rectangular prisms. Thus, the result will not be covered here. Compared with the models with *R/D*=5%, 10%, and 15%, the results for the model with *R/D*=0% show that the wind pressures near the leading edge have stronger correlations with the wind pressures near the trailing edge (see Fig. 21(a)). Meanwhile, the wind pressures near the trailing edge (X>600mm) have weaker correlations with the wind pressures of Point B (see Fig. 21(b)). For rectangular prisms with *R/D*=5%, 10%, and 15%, variations of pressure correlation coefficients between the Point C and the points in the region of X<600 mm are small with a value range of 0 to 0.2. For the rectangular prisms with *R/D*=0%, pressure correlation coefficients between the Point C and the points near X=350 mm obviously decrease (see Fig. 21(c)).

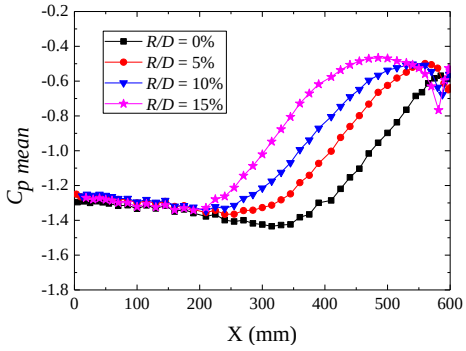

Fig. 18 Mean pressure distributions on the side surfaces of the 3:1 rectangular prisms with various rounded corners

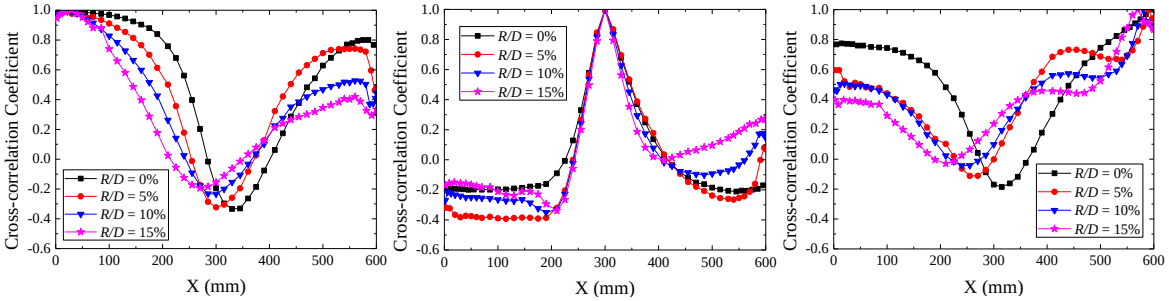

(a) Point A (b) Point B (c) Point C

Fig. 19 Pressure correlation coefficients on the side surfaces of the 3:1 rectangular prisms with respect to various points

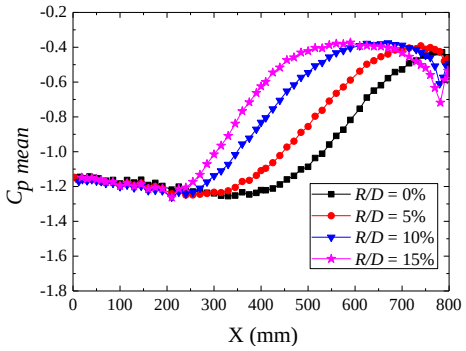

Fig. 20 Mean pressure distributions on the side surfaces of the 4:1 rectangular prisms with various rounded corners

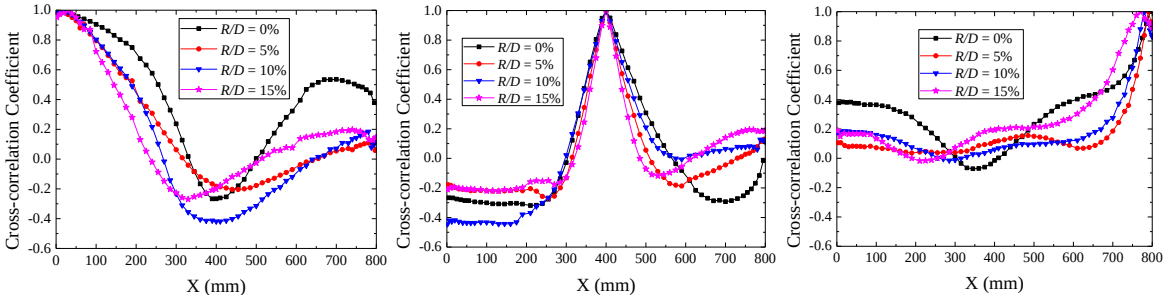

(a) Point A (b) Point B (c) Point C

Fig. 21 Pressure correlation coefficients on the side surfaces of the 4:1 rectangular prisms with respect to various points

5. Conclusions

The Reynolds number effects on the aerodynamic behavior of rectangular prisms with various side ratios and rounded corners have been systematically investigated through wind tunnel experiments. The Reynolds numbers were from 1.1×10^5 to 6.8×10^5, which correspond to the variance of the Reynolds number from the subcritical range to the supercritical range for a 2D circular cylinder. The main findings are summarized as follows:

- Flow reattachment does not occur on the side surfaces of the 2:1 rectangular prisms with $R/D\leq5\%$, whereas the other 10 rectangular prisms undergo complete flow reattachment. However, wind pressure distributions of 12 rectangular prisms are all dependent on the Reynolds number, even if the flow does not reattach to the side surface of the body. For the 3:1 rectangular prisms with $R/D\geq10\%$ and the 4:1 rectangular prisms with $R/D\geq10\%$, a significant influence of the Reynolds number on the mean pressure distributions is observed. These four models exhibit similar behavior, which is characterized by sudden changes in the mean pressure distributions at critical Reynolds numbers.

- According to the variations of the aerodynamic force coefficients with the Reynolds number, rectangular prisms with various rounded corners can be classified into two categories, namely, rectangular prisms with *R/D*=0% and 5% and those with *R/D*=10% and 15%. The aerodynamic force coefficients of the first category gradually change with the Reynolds number, whereas significant changes in aerodynamic force coefficients are observed for the second category at critical Reynolds numbers.
- When $Re=3.4\times10^5$, the rounded corner has a significant influence on the pressure correlations on the side surfaces of the 2:1 rectangular prisms. This phenomenon can be attributed to the separated flow that reattaches to the side surface when $R/D\geq10\%$. For the 3:1 and 4:1 rectangular prisms, the pressure correlations on the side surfaces of rectangular prisms with various rounded corners are similar, and only slight changes are observed with the rounded corner ratio.

Acknowledgments

The authors gratefully acknowledge the supports from the National Natural Science Foundation of China (91215302, 90715040) and Key project of State Key Lab. of Disaster Reduction in Civil Eng. (SLDRCE15-A-04).

References

Carassale, L., Freda, A. and Marrè-Brunenghi, M. (2013),"Effects of free-stream turbulence and corner shape on the galloping instability of square cylinders", *J. Wind Eng. Ind. Aerod.*, **123**, 274-280.

Carassale, L., Freda, A. and Marrè-Brunenghi, M. (2014), "Experimental investigation on the aerodynamic behavior of square cylinders with rounded corners", *J. Fluids Struct.*, **44**, 195-204.

Delany, N.K. and Sorensen, N.E. (1953), "Low-speed drag of cylinders of various shapes", *NACA Technical Note 3038*, Washington, USA.

Gu, M. and Quan, Y. (2004), "Across-wind loads of typical tall buildings", *J. Wind Eng. Ind. Aerod.*, **92**(13), 1147-1165.

Irwin, P.A. (2008), "Bluff body aerodynamics in wind engineering", *J. Wind Eng. Ind. Aerod.*, **96**(6), 701-712.

Kubo, Y., Miyazaki, M. and Kato, K. (1989),"Effects of end plates and blockage of structural members on drag forces", *J. Wind Eng. Ind. Aerod.*, **32**(3), 329-342.

Kwok, K.C.S., Wilhelm, P.A. and Wilkie, B.G. (1988),"Effect of edge configuration on wind-induced response of tall buildings", *Eng. Struct.*, **10**(2), 135-140.

Kwok, K.C.S. (1988), "Effect of building shape on wind-induced response of tall building", *J. Wind Eng. Ind. Aerod.*, **28**(1), 381-390.

Larose, G.L. and D'auteuil, A. (2006), "On the Reynolds number sensitivity of the aerodynamics of bluff bodies with sharp edges", *J. Wind Eng. Ind. Aerod.*, **94**(5), 365-376.

Larose, G.L. and D'Auteuil, A. (2008), "Experiments on 2D rectangular prisms at high Reynolds numbers in a pressurised wind tunnel", *J. Wind Eng. Ind. Aerod.*, **96**(6), 923-933.

Liang, S.G., Liu, S.C., Li, Q.S., Zhang, L.L. and Gu, M. (2002), "Mathematical model of acrosswind dynamic loads on rectangular tall buildings", *J. Wind Eng. Ind. Aerod.*, **90**(12), 1757-1770.

Robertson, J.M., Cermak, J.E. and Nayak, S.K. (1975), "A Reynolds-number effect in flow past prismatic bodies", *Mech. Res. Comm.*, **2**(5), 279-282.

Tamura, T. and Miyagi, T. (1999), "The effect of turbulence on aerodynamic forces on a square cylinder with

various corner shapes", *J. Wind Eng. Ind. Aerod.*, **83**(1), 135-145.
Tamura, T., Miyagi, T. and Kitagishi, T. (1998), "Numerical prediction of unsteady pressures on a square cylinder with various corner shapes", *J. Wind Eng. Ind. Aerod.*,**74**, 531-542.
Tamura,Y., Kim, Y.C., Tanaka, H., Bandi, E.K., Yoshida, A. and Ohtake, K. (2013), "Aerodynamic and response characteristics of super-tall buildings with various configurations", *Proceedings of the 8th Asia-Pacific Conference on Wind Engineering*, Chennai, India.
Tanaka, H., Tamura, Y., Ohtake, K., Nakai, M. and Chul Kim, Y. (2012), "Experimental investigation of aerodynamic forces and wind pressures acting on tall buildings with various unconventional configurations", *J. Wind Eng. Ind. Aerod.*, **107**, 179-191.
Wang, J.M., Cheng, C.M. and Tens, P.T. (2003), "Design wind loads on tall buildings: a wind tunnel data based expert system approach", *Proceedings of the 11th International Conference on Wind Engineering*. Lubbock, TX, USA.
Xie, J.M. (2014), "Aerodynamic optimization of super-tall buildings and its effectiveness assessment", *J. Wind Eng. Ind. Aerod.*, **130**, 88-98.

CC